Received: 22 May 2021 | Revised: 22 July 2021 | Accepted: 2 August 2021

DOI: 10.1002/aoc.6412

RESEARCH ARTICLE

Applied Organometallic Chemistry WILEY

Synthesis, characterization, biological evaluation, and molecular docking approach of nickel (II) complexes containing O, N-donor chelation pattern of sulfonamide-based Schiff bases

Ahmed M. Ramadan[1] | **Hoda A. Bayoumi**[2] | **Rehab M. I. Elsamra**[1]

[1]Chemistry Department, Faculty of Science, Alexandria University, Alexandria, Egypt

[2]Chemistry Department, Girls College for Arts, Science and Education, Ain-Shams University, Cairo, Egypt

Correspondence
Ahmed M. Ramadan, Chemistry Department, Faculty of Science, Alexandria University, P.O. Box 426, Alexandria 21321, Egypt.
Email: ahmed.m.ramadan@alexu.edu.eg

Abstract

A series of Schiff bases (L^1–L^4) that possess in their structure bioactive sulfonamide group and their nickel (II) complexes have been synthesized. Microanalytical analyses, various spectroscopic methods such as Fourier transform infrared spectroscopy (FT-IR), ^{1}H nuclear magnetic resonance (NMR), ^{13}C NMR, UV–Vis, and MS, are used to explore the nature of bonding and to elucidate the chemical structures. The analytical and magnetic values suggest a range of stoichiometries 1:1, 1:2, and 2:1 (M:L) for the synthesized complexes of almost square planar geometry. The spectral comparative interpretation reveals that L^1 and L^2 coordinate to the central Ni (II) in tetradentate ONON donor sequence, whereas L^3 and L^4 in bidentate ON pattern through deprotonated phenolic-O and the azomethine-N. Density functional theory (DFT) and MOE-docking approaches are used to evaluate the molecular parameters and the binding propensity of the synthesized ligands and their complexes with 3s7s protein and to signify their inhibition strength. Besides, the anticancer, antimicrobial and antifungal activities have been screened against number of tumor cells and human pathogen strains. These in vitro studies reveal that Schiff base L^4 and its complex, [Ni(L^4-H)(OAc)(H_2O)], have superior activities reflecting the importance of inserting bioactive pendant substituents such as thiazole ring and 3-fluorophenylazo to the pharmacophoric sulfonamide moiety. Moreover, some of the synthesized Ni (II) complexes display promising therapeutic effects as novel non-platinum antitumor agents after further preclinical investigations.

KEYWORDS

anticancer efficacy, antimicrobial activity, coordination modes, DFT calculations, sulfa drugs

1 | INTRODUCTION

Schiff bases are privileged compounds owing to their wide range of biological activities and industrial applications.[1–3] They can be synthesized simply by condensation of primary amines and aldehydes forming azomethine moiety. Structural resemblances of these compounds with natural biological molecules have

evoked versatile pharmacological performances including anti-inflammatory, antiviral, antibacterial, antifungal, wound healing, and nerve breakdown protection.[2–5] Also, the metal complexes of Schiff bases are known for their free radicals scavenging power protecting living cells from the adverse consequences of these radicals.[6,7] For decades, there are a growing number of researches in the area of complexation of Schiff base derivatives with various donor N, O, and S atoms especially those containing sulfa drug units. The main objective of most of these efforts is to increase the synergistic properties of Schiff base ligands by combination of different bioactive moieties such as sulfonamide, acyl pyrazolones, and diazenyl linkages.[7–9] Besides, there is an increasing consideration for synthesis and development of novel non-platinum metal complexes to overcome the unresolved clinical complications associated with using carboplatin or cisplatin in cancer treatment.[10,11] Recently, there is an increasing demand for designing potentially effective anti-pathogenic and anti-COVID-19 agents to overcome the developed resistance of many microbes and viruses attacking human.[12,13] Toward achieving these goals herein presented the synthesis, characterization of newly Ni (II) complexes derived from Schiff base ligands whose structures contain combination of 3-fluorophenylazo, sulfonamide, and/or thiazole substituents.

2 | EXPERIMENTAL

2.1 | Materials, instruments, and methodology

The purity of the compounds was checked by precoated TLC plates (MERCK) using chloroform: methanol (7:3) mixture. All the chemical materials used are of analytical reagent grade and used without further purifications. 3-Fluoroaniline, Ni $(OAc)_2.4H_2O$, sulfanilamide (SNM), and sulfathiazole (STZ) were purchased from Sigma–Aldrich and Fluka companies. All solutions used throughout the experiments were prepared freshly in ultrapure water obtained from ultrapure water system in which water was distilled and deionized. Gallenkamp MFB-595 device was utilized to record melting points. IR spectra were recorded using KBr disc method on Fourier transform infrared spectroscopy (FT-IR) Bruker tensor 37 within 400–4000 cm^{-1} spectral range. Mass spectra were recorded on Shimadzu Qp-2010 plus mass spectrometer at 70 eV, Faculty of Science, Cairo University. The nuclear magnetic resonance (NMR) spectra (^1H, 500 MHz; ^{13}C, 125 MHz) were recorded at room temperature using Bruker AC-500 spectrometer. Chemical shifts are expressed in δ (ppm) with tetramethylsilane (TMS) as the reference. For Ni (II) complexes, the metal content was estimated by convenient indirect titration with standard EDTA,[14] and by atomic absorption technique at the central lab, Alexandria University. Simultaneous thermal analyses (TGA/DTGA) of the nickel complexes were carried out at heating rate 10°C min^{-1} using Bruker LINSEIS STA PT 1000 under N_2 flow of 20 cm^3 min^{-1}. GAUSSIAN 09 software was used for the calculations of molecular orbital parameters based on the density functional theory (DFT)(B3LYP/6-31G) level of theory. The optimized structures were visualized in GAUSSIAN-VIEW.[15] Optimization was achieved without constraining the geometry of the inspected compounds. Docking investigation was attained by MOE 2015.10 software. The intial steps to prepare the tested compound for the docking process included hydrogen atoms addition, removal of water molecules, atomic charges clarifying and then energy minimization by MMFF94x force field.[16] The inhibition strength was deduced from the magnitude of scoring energy and the number of effective ligand-protein bonds in the simulated poses.[17]

2.2 | Antibacterial, antifungal and anticancer activities

Compounds (L^1–L^4) were tested in vitro for their antimicrobial activities by agar diffusion method as previously described.[18] The utilized organisms were two Gram-positive bacteria (*Streptococcus pneumoniae* and *Bacillus subtilis*), two Gram-negative bacteria (*Pseudomonas aeruginosa* and *Escherichia coli*), and two fungal strains (*Aspergillus fumigatus* and *Candida albicans*). The observed mean zone diameter of inhibition in mm is considered as an index of the antimicrobial activity of the tested samples. Besides, the minimal inhibitory concentration (MIC, μg/ml) was estimated by applying broth microdilution assay as previously depicted in a study conducted by our group.[19] Ampicillin, gentamycin, and amphotericin B were used as standard references for antibacterial and antifungal activities.

In addition, the synthesized ligands and some selected nickel (II) complexes were preliminarily assessed for their anticancer efficacy against human hepatocellular carcinoma cells (HepG-2), colon carcinoma cells (HCT-116), and breast carcinoma cells (MCF-7) by crystal violet viability method as described.[20] Cisplatin and imatinib were utilized as positive controls under the same assessment conditions. Furthermore, some compounds were evaluated against oral epithelial cell line (OEC) to gauge their toxicity on normal cells under the same assay conditions. OEC cell line (PCS-200-014) was obtained from the American Type Culture Collection

(ATCC, Rockville, MD). Antimicrobial and cytotoxicity evaluations were performed by Regional Center for Mycology & Biotechnology (RCMP) at Al-Azhar University, Cairo, Egypt.

2.3 | Synthesis of 5-(3-fluorophenylazo) salicylaldehyde (3-FAS)

The newly 3-FAS compound was prepared by the usual diazotization process (Scheme 1).[21] The required 3-fluoroaniline (0.05 mole, $d = 1.156$, 4.8 ml) in 15-ml HCl (37%) was diazotized below 5°C with a solution of $NaNO_2$ (0.05 mole, 3.45 g) and 20-ml distilled water. The diazonium chloride was coupled with an alkaline solution of salicylaldehyde (0.05 mole, $d = 1.1655$, 5.23 ml). The crude dye was filtered, washed with distilled H_2O, and dried in vacuum over P_4O_{10}, ($C_{13}H_9N_2O_2F$ Yellow color, m.p. 140–142°C).

2.4 | General method for the synthesis of a series of Schiff base ligands (L^1–L^4)

The Schiff base ligands were prepared by reaction of equimole (10 mmole) of sulfa drug (SNM or STZ) with salicylaldehyde or substituted salicylaldehyde (3-FAS).[22]

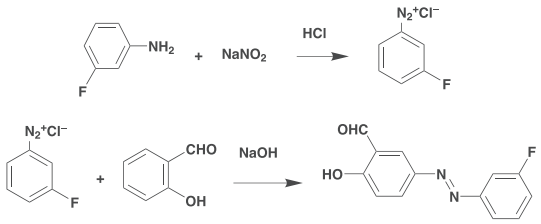

SCHEME 1 Synthesis of 5-(3-fluorophenylazo)salicylaldehyde (3-FAS)

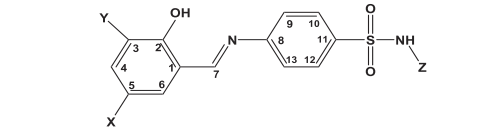

Schiff base	X	Y	Z
L^1	H	H	H
L^2	H	H	
L^3	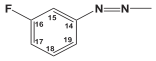	H	H
L^4	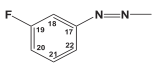	H	

SCHEME 2 Structures of Schiff base ligands (L^1–L^4)

Each reactant was dissolved in a minimum amount of ethanol and followed by addition of 2-ml glacial acetic acid. The solution was refluxed for 8 h then cooled to room temperature and poured into ice cold water. The isolated colored Schiff bases (Scheme 2) were collected through filtration and then dried using drying oven at 80°C. The products were purified by repeated recrystallization in ethanol/H_2O solvents and then dried.

2.4.1 | 4-([2-Hydroxybenzylidene]amino)-benzenesulfonamide (L^1)

Bright yellow crystals, yield (73%), m.p. 208–209°C; UV–Vis. (DMF) λ_{max}/nm: 232, 273, 342; IR (KBr) ν_{max}/cm^{-1}: 3341 ν_{asym} (NH_2), 3245 ν_{sym} (NH_2), 3,060 ν (OH), 3,028 ν (CH-sp^2), 1,617 ν(C=C), 1571 ν(C=N), 1368 ν_{asym} (SO_2), 1182 ν_{sym} (SO_2); ^{1}H NMR (500 MHz, DMSO-d_6): $\delta_{ppm} = 12.65$ (1H, s, OH); 9.00 (1H, s, C_7-H); 7.90 (2H, d, C_{10}-H, C_{12}-H); 7.71 (1H, d, C_6-H); 7.57 (2H, d, C_9-H, C_{13}-H); 7.47 (1H, t, C_4-H); 7.42 (2H, s, NH_2); 7.02 (1H, d, C_5-H); 7.00 (1H, d, C_3-H); ^{13}C-NMR (500 MHz, DMSO-d_6): $\delta_{ppm} = 116.7$ (C_3); 119.3 (C_1); 119.4 (C_5); 121.8 (2C, C_9, C_{13}); 127.4 (2C, C_{10}, C_{12}); 132.5 (C_6); 133.9 (C_4); 142.0 (C_{11}); 151.2 (C_8); 160.2 (C_7H=N); 164.9 (C_2-OH); 276 (M^+, 100); 212 (19.10); 195 (90.5); 167 (33.4); 108 (39.1); 92 (60.4); 77 (33.5); 65 (76.1); 51 (30.2); Anal. Calcd. for $C_{13}H_{12}N_2O_3S$ (276.31): C, 56.51.28; H, 4.38; N, 10.14; S, 11.60%, Found: C, 56.73; H, 4.25; N, 9.96; S, 11.79%.

2.4.2 | 4-([2-Hydroxybenzylidene]amino)-*N*-(1,3-thiazol-2-yl)benzenesulfonamide (L^2)

Golden yellow crystals, yield (82%), m.p. 218–220°C; UV–Vis. (DMF) λ_{max}/nm: 279, 345; IR (KBr) ν_{max}/cm^{-1}: 3145 ν (NH), 3115, 2800 ν (OH), 3017 ν (CH-sp^2), 1616 ν(C=C), 1580, 1532 ν(C=N), 1362 ν_{asym} (SO_2), 1182 ν_{sym} (SO_2); ^{1}H NMR (500 MHz, DMSO-d_6): $\delta_{ppm} = 12.59$ (1H, s, OH); 10.75 (1H, s, NH); 8.97 (1H, s, C_7-H); 7.87 (2H, d, C_{10}-H, C_{12}-H); 7.69 (1H, d, C_{15}-H); 7.52 (2H, d, C_9-H, C_{13}-H); 7.45 (1H, t, C_4-H); 7.29 (1H, d, C_6-H); 7.00 (1H, t, C_5-H); 6.86 (1H, d, C_3-H); 6.56 (1H, d, C_{16}-H); ^{13}C-NMR (500 MHz, DMSO-d_6): $\delta_{ppm} = 108.3$ (C_{16}); 116.7 (C_3); 117.2 (C_1); 119.3 (C_5); 121.8 (2C, C_9, C_{13}); 127.7 (2C, C_{10}, C_{12}); 129.2 (C_6); 132.5 (C_4); 136.4 (C_{15}); 140.1 (C_{11}); 151.4 (C_8); 160.7 (C_7H=N); 165.0 (C_2-OH); 168.9 (C_{14}); MS m/z (%): 359 (M^+, 26.6); 295 (24.5); 196 (100); 176 (62.6); 167 (24.9); 99 (9.44); 92 (13.0); 77 (22.0); 65 (16.9); 51 (18.6); Anal. Calcd. for $C_{16}H_{13}N_3O_3S_2$ (359.42): C, 53.47; H, 3.65; N, 11.69; S, 17.84%, Found: C, 53.58; H, 3.55; N, 11.54; S, 18.01%.

2.4.3 | 4-((5-[3-fluorophenylazo]-2-hydroxybenzylidene)amino)-benzene-sulfonamide (L^3)

Red powder, yield (61%), m.p. 206–208°C; UV–Vis. (DMF) λ_{max}/nm: 408, 465; IR (KBr) ν_{max}/cm^{-1}: 3364 ν_{asym} (NH_2), 3261 ν_{sym} (NH_2), 3075 ν (OH), 3029 ν (CH-sp^2), 1619 ν(C=C), 1,570 ν(C=N), 1493 ν(N=N), 1334 ν_{asym} (SO_2), 1153 ν_{sym} (SO_2); ^{1}H NMR (500 MHz, DMSO-d_6): δ_{ppm} = 11.71 (1H, s, OH); 9.17 (1H, s, C_7-H); 8.38 (1H, s, C_6-H); 8.22 (1H, s, C_{15}-H); 8.11 (1H, d, C_4-H); 7.93 (1H, d, C_{19}-H); 7.77 (1H, t, C_{18}-H); 7.64 (2H, d, C_{10}-H, C_{12}-H); 7.43 (2H, d, C_9-H, C_{13}-H); 7.21 (1H, d, C_{17}-H); 6.89 (2H, s, NH_2); 6.59 (1H, d, C_3-H); ^{13}C-NMR (500 MHz, DMSO-d_6): δ_{ppm} = 107.4 (C_{15}); 107.5 (C_3); 112.4 (2C, C_9, C_{13}); 117.6 (C_1); 119.6 (C_{17}); 121.8 (C_{19}); 122.7 (C_6); 124.1 (C_4); 127.4 (2C, C_{10}, C_{12}); 129.9 (C_{18}); 131.2 (C_{11}); 142.3 (C_5); 144.6 (C_{14}); 150.8 (C_8); 153.5 (C_7H=N); 163.7 (C_{16}-F); 163.9 (C_2-OH); MS m/z (%): 398 (M^+, 49.1); 275 (39.3); 215 (1.9); 198 (1.4); 195 (77.1); 167 (59.3); 123 (7.6); 95 (100); 93 (10.6); 77 (11.7); 65 (68.7); Anal. Calcd. for $C_{19}H_{15}FN_4O_3S$ (398.41): C, 57.28; H, 4.77; N, 14.06; S, 8.05%, Found: C, 57.35; H, 4.55; N, 13.91; S, 8.16%.

2.4.4 | 4-((5-[3-fluorophenylazo]-2-hydroxybenzylidene)amino)-*N*-(1,3-thiazol-2-yl)-benzene-sulfonamide (L^4)

Orange powder, yield (71%), m.p. 236–237°C; UV–Vis. (DMF) λ_{max}/nm: 406, 468; IR (KBr) ν_{max}/cm^{-1}: 3135 ν (NH), 3092, 2801 ν (OH), 3020 ν (CH-sp^2), 1619 ν(C=C), 1568, 1539 ν(C=N), 1481 ν(N=N), 1329 ν_{asym} (SO_2), 1143 ν_{sym} (SO_2); ^{1}H NMR (500 MHz, DMSO-d_6): 13.26 (1H, s, OH); 12.54 (1H, bs, NH); 9.12 (1H, s, C_7-H); 8.36 (1H, s, C_6-H); 8.06 (1H, d, C_4-H); 7.89 (1H, d, C_{22}-H); 7.77 (1H, d, C_{15}-H); 7.66 (1H, d, C_{18}-H); 7.63 (1H, t, C_{21}-H); 7.58 (2H, d, C_{10}-H, C_{12}-H), 7.29 (1H, d, C_{20}-H); 7.19 (2H, d, C_9-H, C_{13}-H); 6.86 (1H, d, C_3-H); 6.56 (1H, d, C_{16}-H); ^{13}C-NMR (500 MHz, DMSO-d_6): δ_{ppm} = 107.3 (C_{18}); 107.5 (C_{16}); 112.4 (2C, C_9, C_{13}); 117.6 (C_3); 117.8 (C_1); 118.4 (C_{20}); 120.1 (C_{22}); 122.5 (C_6); 124.3 (C_4); 127.7 (2C, C_{10}, C_{12}); 129.9 (C_{21}); 131.2 (C_{15}); 131.3 (C_{11}); 144.5 (C_5); 152.1 (C_{17}); 153.3 (C_8); 153.4 (C_{19}-F); 161.7 (C_7H=N); 163.6 (C_2-OH); 168.9 (C_{14}); MS m/z (%): 481 (M^+, 61.3); 398 (2.3); 318 (38.8); 215 (3.8); 198 (1.4); 123 (6.1); 95 (100); 93 (19.5); 77 (12.7); 65 (76.5); Anal. Calcd. for $C_{22}H_{16}FN_5O_3S_2$ (481.52): C, 54.88; H, 3.35; N, 14.54; S, 13.32%, Found: C, 55.09; H, 3.25; N, 14.47; S, 13.41%.

2.5 | General procedure for the synthesis of nickel (II) complexes

A solution of Ni $(CH_3COO)_2.4H_2O$ (2.49 g, 10 mmol) in EtOH (10 ml) was added to a stirred solution of Schiff base (L^1-L^4) (5 mmol) in hot EtOH (25 ml). Few drops of DMF was added to help the solubility of the Schiff base before mixing. Then, NaOAc (0.41 g, 5 mmol) dissolved in least amount of H_2O was added to make the medium slightly basic. The mixture was heated at 60°C for 1 h under stirring. The precipitated complex was filtered and washed with MeOH, and then air dried. The analytical and physical properties of the synthesized metal complexes were collected in Table 1.

3 | RESULTS AND DISCUSSION

3.1 | Structure elucidation of the synthesized Schiff base ligands (L^1–L^4) and their complexes

The synthesized sulfonamide-based Schiff bases (L^1–L^4) showed a considerable ability to form chelates with diverse stoichiometric ratios (Table 1) 1:1, 1:2 or 2:1 (M:L). This coordination capability is attributed to the presence of many binding sites (oxygen, nitogen, and sulfur atoms) (Scheme 2).

3.1.1 | Fourier transform infrared spectroscopy, nuclear magnetic resonance, MS, and coordination modes

Microanalytical and various spectroscopic methods such as FT-IR, ^{1}H NMR, ^{13}C NMR, and MS, (Table 1 and Figure 1), were used in order to assign the chemical structures of the synthesized compounds. Full interpretations of all spectral data are elaborated in Section 2 and in the supporting information (Table S1 and Figures S1–S13). Characteristic infrared spectral band of the precursor 3-FAS appeared at 1478 cm^{-1} due to ν(N=N) (Figure S1) indicating the formation of the azo derivative from the reaction of 3-fluoroaniline with salicylaldehyde (Scheme 1). Also, the sharp strong band in the IR spectrum of 3-FAS at 1671 cm^{-1} corresponding to ν(C=O) was disappeared in the ligand's spectra (Figures 1 and S2) inferring Schiff condensation with sulfanilamide (SNM) or sulfathiazole (STZ) (Scheme 2). Besides, the synthesized Schiff base ligands (L^1–L^4) showed a new strong to moderate band in the range 1568–1580 cm^{-1} assigned to azomethine ν (HC=N) linkage.[23] Further, the twin broad bands in the IR

TABLE 1 Analytical data and physical properties for nickel (II) complexes

	Complex (M:L)	Formula Color Color	% Calculated/ (Found) M	C	H	N	S	μ_{eff} B.M	Λ_m $\Omega^{-1}mol^{-1}cm^2$
(1)	$[Ni_2(L^1\text{-}H)(OAc)_3(H_2O)].H_2O$	$C_{19}H_{24}N_2O_{11}SNi_2$	19.38	37.67	3.99	4.62	5.29	0.71	3.45
	(2:1)	Brown	(19.38)	(37.82)	(4.09)	(4.76)	(5.19)		
(2)	$[Ni_2(L^2\text{-}H)(OAc)_3(H_2O)]$	$C_{22}H_{23}N_3O_{10}S_2Ni_2$	17.50	39.38	3.46	6.26	9.56	0.59	1.90
	(2:1)	Reddish brown	(17.42)	(39.51)	(3.58)	(6.32)	(9.40)		
(3)	$[Ni(L^3\text{-}H)_2].4H_2O$	$C_{38}H_{36}F_2N_8O_{10}S_2Ni$	6.34	49.31	3.92	12.11	6.93	dia.	2.45
	(1:2)	Dark orange	(6.12)	(49.51)	(4.06)	(12.36)	(6.71)		
(4)	$[Ni(L^4\text{-}H)(OAc)(H_2O)]$	$C_{24}H_{20}FN_5O_6S_2Ni$	9.52	46.77	3.27	11.36	10.41	0.71	1.63
	(1:1)	Brown	(9.34)	(46.82)	(3.41)	(11.48)	(10.28)		

Note: All complexes have m.p. > 300°C.

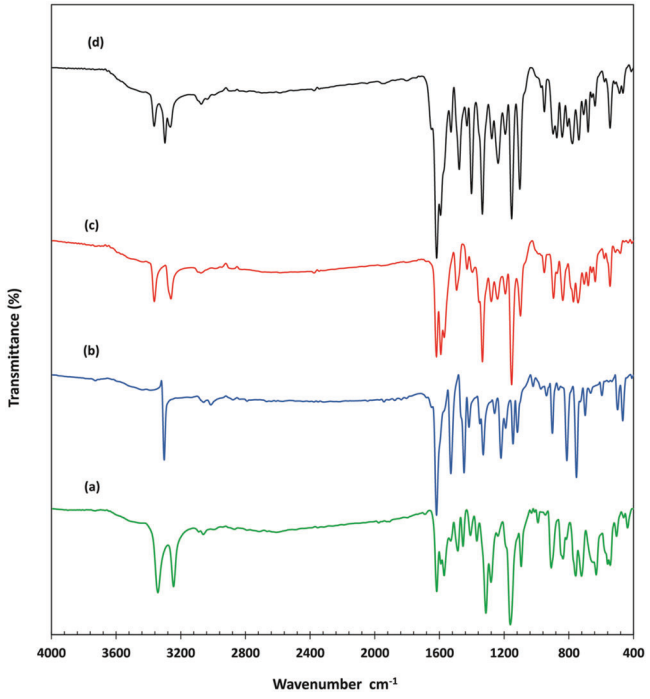

FIGURE 1 FT-IR of (a) L^1, (b) $[Ni_2(L^1\text{-}H)(OAc)_3(H_2O)].H_2O$, (c) L^3, (d) $[Ni(L^3\text{-}H)_2].4H_2O$

spectra of L^1 and L^3 in the range 3245–3364 cm^{-1} typified the asymmetric and symmetric stretching vibrations of NH_2 of the sulfonamide group (Figure 1). Nevertheless, the IR spectra of the free ligands L^2 and L^4 showed various bands at 2800–3145 cm^{-1} assigned to νNH of sulfonamide and νOH of the phenolic group (Figure S2). The appearance of OH stretching modes at lower frequencies than its ordinary position (~3300–3400 cm^{-1}) could be attributed to intramolecular hydrogen-bonding (O–H---N) with the neighbor azomethine group.[24] Moreover, the two bands that appeared at 1329–1368 and 1143–1182 cm^{-1} were correspondingly assigned to the vibrations ν_{asym} (SO_2) and ν_{sym} (SO_2) (Table S1).

A comparative analysis of the IR spectra of the Schiff base ligands (L^1–L^4) and their nickel complexes sheds light to specify the bonding mode of the surrounding ligands with the central Ni (II) ion. There are some guide bands which assist in achieving this target. For instance, the band ν (CH=N) in the spectra of all free ligands is considerably lowered in frequency (~15 cm^{-1}), weakened and appeared as shoulder in the spectra of all complexes (Table S1 and Figures 1 and S2) implying the involvement of azomethine nitrogen atom in coordination.[25] Also, the phenolic νOH is vanished in the spectra of all complexes supporting its participation in coordination after deprotonation.[26]

In case of complexes (**1**) and (**2**) of the type (M_2L), the asymmetric stretching band due to the sulfonyl group ($\nu_{asym}SO_2$) is shifted to lower frequency (33–39 cm^{-1}) compared to the free ligands L^1 and L^2 (Table S1) proposing sulfonyl oxygen as an additional coordination site in these cases. This is accompanied by disappearance of either the twin bands of ν (NH_2) or ν (NH) in case of L^1 and L^2, respectively, substantiating the enolization process of the sulfonamide group SO_2NH (H) to SO (OH) = N(H) before coordination as reported by previous studies of metal-sulfa drugs based chelates of a dinuclear feature (M_2L).[27,28] Accordingly, there is an interaction between the metal ion with the sulfonamidic-N and sulfonyl-O atoms of L^1 through four-membered ring formation in case of complex (**1**).[29,30] As well, the blue shift and the weakness of the ν(C=N) at 1532 cm^{-1} of the thiazole moiety of L^2 in the spectra of its complex (**2**) favoring the chelation of the thiazole-N atom to give more stable six-membered ring.[28,31] Unlikely, there is no remarkable change of the sulfonamide group vibrational modes in case of L^3 and L^4 complexes (**3**) and (**4**) (Table S1) ruling out its participation in coordination with Ni (II) in these cases.

Therefore, it is concluded that the ligands are chelated to the metal ion in two different ways by one or two bidentate (ON) donor atoms. L^1 and L^2 both behave as a monobasic tetradentate (ONON) donor sequence as coordinated to the Ni (II) ion via deprotonated phenolic-O, the azomethine-N, enolic sulfonamide S(O)OH, sulfonamidic-N or thiazole-N (Scheme 3). However, L^3 and L^4 coordinate in a monobasic bidentate fashion (ON) by only deprotonated phenolic-O and the azomethine-N. It is worth mentioning that different complexes of L^1 and L^2 with different stoichiometry (ML_2) have been isolated in previous studies.[25,32] In these researches, they were bound to the central metal ion as neutral bidentate ligands and not in the deprotonated tetradentate fashion (M_2L) as in our case. This could be attributed to the difference in the pH of the medium during preparation and the type of the counter anions.[32]

Additionally, the emergence of two new bands in the ranges 1398–1447 and 1219–1231 cm^{-1} in the spectra of complexes (**1**), (**2**), and (**4**) characteristic of the asymmetric and symmetric stretching vibrations of the COO^- group, respectively, points to a monodentate pattern of the acetate group around the metal ion.[33] Also, the low frequency bands that are only observable in the spectra of the metal complexes in 529–595 and 466–481 cm^{-1} regions due to ν(M-O) and ν(M-N) assert the complex formation.[31]

Likewise, ^{1}H NMR and ^{13}C NMR spectral data of the synthesized ligands (L^1–L^4) have provided additional support to their structures (Figures S3–S7). In particular, the OH group at C(2) was found in the range δ 11.71–13.26 ppm as a D_2O-exchangeable singlet peak in the ^{1}H NMR spectra of all ligands (Figures S4 and S5). Also, the two NH_2 protons of the sulfonamide group of L^1 and L^3 were located as strong singlet peak at 7.42 and 6.89 ppm, respectively, inside the aromatic range δ 6.58–8.39 ppm (Figure S3). However, the singlet peak of NH proton in the case of L^2 and L^4 was appeared in the downfield region at δ 10.75 and 12.54 ppm (Figure S4), respectively. As for ^{13}C NMR, the compound L^4, $C_{22}H_{16}FN_5O_3S_2$, displayed 20 distinct types of carbons (Figure S7) among which two lines having integration of two carbons of an identical environment at 112.4 ppm (C_9, C_{13}) and 127.7 ppm (C_{10}, C_{12}). Besides, the key peaks at δ 161.7, 163.6, and 168.9 ppm were attributed to azomethine (C_7H=N), C_2-OH and thiazole (C_{14}) carbons (Scheme 2). The proposed mode of binding was further scrutinized by NMR spectral comparison of L^3 and its diamagnetic Ni (II) complex (**3**) (Figure S3). The phenolic OH signal at δ 11.71 ppm in the spectra of the free ligand (Figure S3a) is disappeared in complex (**3**) (Figure S3b) endorsing the deprotonation of the OH group at C(2) before coordination. The existence of electron withdrawing substituents azo (N=N) at C(5) and F atom at C(16) in the adjacent phenyl moiety may ease this proton removal at C (2) (Scheme 2). On the other hand, the singlet NH_2 protons peak at δ 6.89 ppm is nearly unchanged in both ligand and complex (**3**) spectra (Figure S3b) overruling any interaction of Ni (II) ion and the amino group of the sulfonamide part.[30]

Based on the mass spectral data, the molecular ion peaks ($\mathbf{M}^{+\bullet}$) of the synthesized Schiff base ligands (Figures S8 and S9) are in good consistency with their formula weights. Scheme 4 represents the proposed fragmentation pattern of L^4 as a descriptive example. Also, the complexes (**1**) to (**4**) displayed ($M^{+\bullet}$) at m/z = 605.94, 671.12, 926.29, and 616.76, respectively, that adequately support their elucidated chemical structures by other analytical and spectral techniques (Figures S10–S13). In this regard, the mass spectrum of the dinuclear complex (**1**), $[Ni_2(L^1\text{-}H)(OAc)_3(H_2O)].H_2O$, exposed a prominent peak at m/z 276.25 (100%) corresponding to the molecular ion peak of its precursor L^1 (Figure S10). The spectrum also displayed a group of peaks at m/z 588.27, 569.72, 510.99, and 329.47 corresponding to dinuclear cation fragments $[Ni_2(L^1\text{-}H)(OAc)_3(H_2O)]$, $[Ni_2(L^1\text{-}H)(OAc)_3]$, $[Ni_2(L^1\text{-}H)(OAc)_2]$, and $[Ni_2(L^1\text{-}H)]$, respectively. Besides, the peaks at m/z 453.09, 392.47, 334.08, and 117.92 could be assigned to the mononuclear cations $[Ni(L^1\text{-}H)(OAc)_2]$, $[Ni(L^1\text{-}H)(OAc)]$, $[Ni(L^1\text{-}H)]$, and [Ni (OAc)] in sequence. Similarly, the complex $[Ni(L^4\text{-}H)(OAc)(H_2O)]$ (**4**) gives monomeric cationic fragments $[Ni(L^4\text{-}H)(OAc)]$, $[Ni(L^4\text{-}H)]$, and [Ni (OAc)] at m/z = 598.77, 540.36, and 117.74 (Figure S13) upon losing bulky molecular ions from the inner sphere. Also, the loss of 3-fluorophenylazo moiety from L^4 molecule in $[Ni(L^4\text{-}H)(OAc)]$ (**4**) leads to the appearance of L^2 peak at m/z = 359.46 in the spectra of complex (**4**), Figure S13. Interestingly, the appearance of a peak at $m/z \cong 59$ in all complexes coincides with the existence of nickel isotope supporting the complexation process.[34]

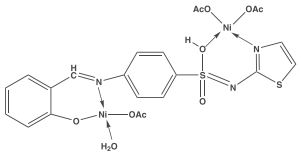

SCHEME 3 Structure of $[Ni_2(L^2\text{-}H)(OAc)_3(H_2O)]$ complex (**2**)

3.1.2 | UV–Vis, conductivity, and magnetism measurements

The electronic spectra of L^1–L^4 series have been recorded in DMF solvent where absorptions curves of two or three

SCHEME 4 Mass fragmentation pattern of L^4

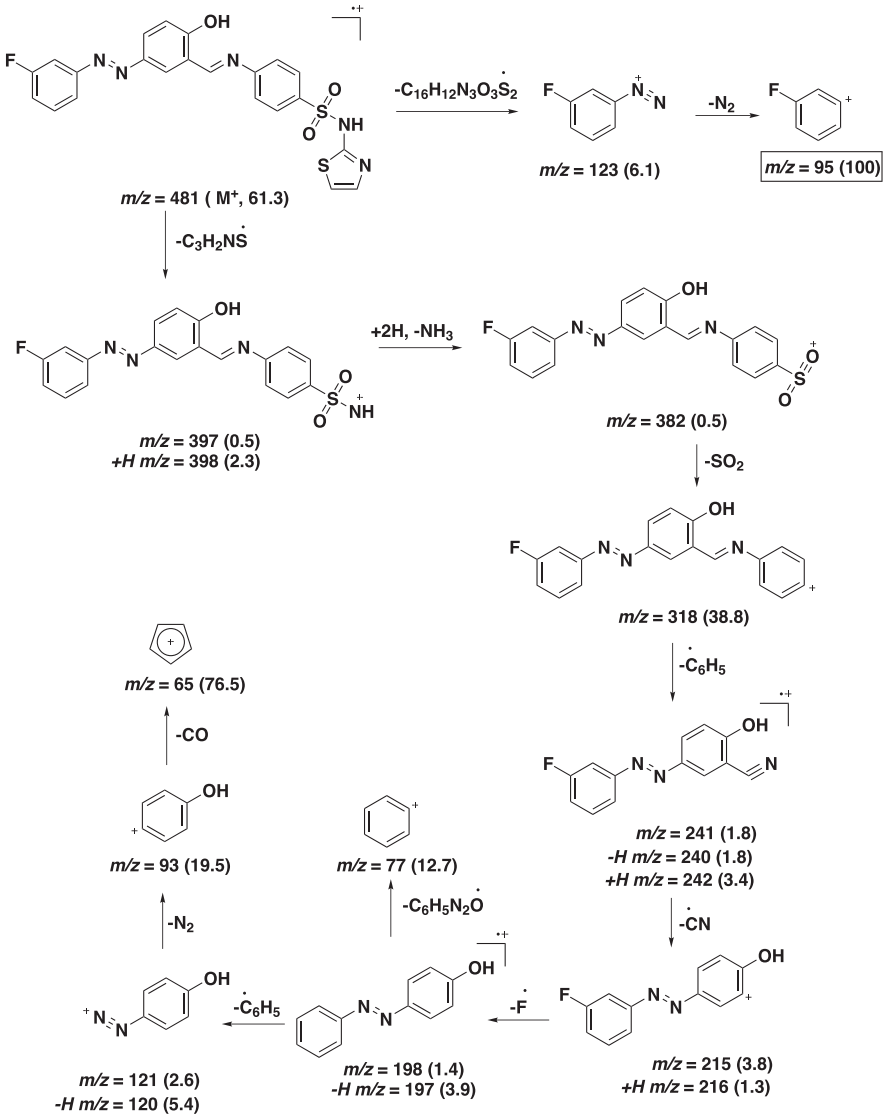

bands within the ranges 232–279, 342–345, and 406–468 nm were noticed. The bands are related to $\pi \rightarrow \pi^*$ and $n \rightarrow \pi^*$ transitions due to a comparatively long-conjugated system in the ligand's structure especially in the case of L^3 or L^4 where three phenyl groups are linked by azo and azomethine bridges. Also, the ligands possess several atoms bearing nonbonding electrons such as oxygen, nitrogen and sulfur atoms (Scheme 2). Similar absorption bands were obtained in case of complexes with obvious broadening up to ~500 nm. The broad feature in this region could be related to charge transfer of LMCT type that makes it difficult to detect any weak d–d transitions inside the metal ion.[35]

The molar conductance (Λ_m) of the complexes in DMF at a concentration of 1×10^{-3} M was recorded in the range 1.63–3.45 Ω^{-1} mol^{-1} cm^2 (Table 1) supporting their non-electrolytic behavior and neutrality of the coordination sphere.[28] The magnetic susceptibility values (μ_{eff}) at 296 K of the Ni (II) complexes (**1**), (**2**), and (**4**) are in the range 0.59–0.71 B. M (Table 1) signifying the existence of square planar ↔ tetrahedral geometries in the same solid phase.[36] The tetrahedral percentage (N_t) in this 4-coordinate mixture could be calculated by using the equation: $N_t = [(\mu_{obs.})^2/(3.3)^2] \times 100$, where μ_{obs} is the observed room temperature magnetic moment and 3.3 is the value of magnetic moment in case of perfect tetrahedral Ni (II) complexes.[37] Thus, the N_t values of complexes (**1**), (**2**), and (**4**) lies in the range of 3.20%–4.63%. The low N_t value hints at the bulkiness effect of the substituents on phenyl moieties that favors square planar shape.[37] Nevertheless, the zero μ_{eff} value for Ni (II) complex (**3**) approves its adopted square-planar geometry with diamagnetic features. Moreover, the later finding proposes that the two sulfonamide-based ligand (L^3) molecules in complex (**3**) are being strong enough to produce a considerable ligand-field splitting factor enhancing the planar form.[38]

3.1.3 | Thermal studies

The thermal properties of nickel complexes derived from Schiff bases (L^1–L^4) were dissected using TGA and DTGA methods under N_2 gas flow up to ~800°C (Figures 2 and 3). All thermal peaks details, the percentage of mass losses and their assignments are listed in Table 2. As an illustrating example, the thermal decomposition of the $[Ni_2(L^2\text{-H})(OAc)_3(H_2O)]$ complex (**2**) proceeds in three stages (Figure 2). The first stage at temperature range ~74–297°C is corresponding to the combined loss of one H_2O and one CH_3COOH molecule from the inner coordination sphere (calc. 11.6%; found 11.4%). The second stage points to the decarboxylation process of two chelated acetate groups accompanied with the starting of ligand decomposition in the temperature range ~297–380°C. The mass loss continues in the third stage which is related to the bulk of the ligand fragment ($C_{16}H_9N_3OS_2$) up to 523°C (Table 2) leaving 2 NiO as a residue (calc. 22.3%; found 22.3%). The variation between the found and calculated mass losses in second and third stages is taken as an indication of overlapping of the decomposition steps in these stages. Also, the two NiO residual composition is in conformity with the proposed dinuclear structure of complex (**2**) as reported for analogous Schiff bases complexes.[39]

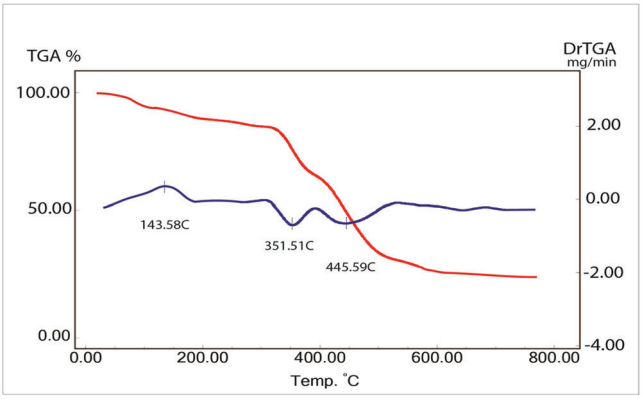

FIGURE 2 TGA and DTGA of $[Ni_2(L^2\text{-H})(OAc)_3(H_2O)]$ complex (**2**) under N_2 atmosphere

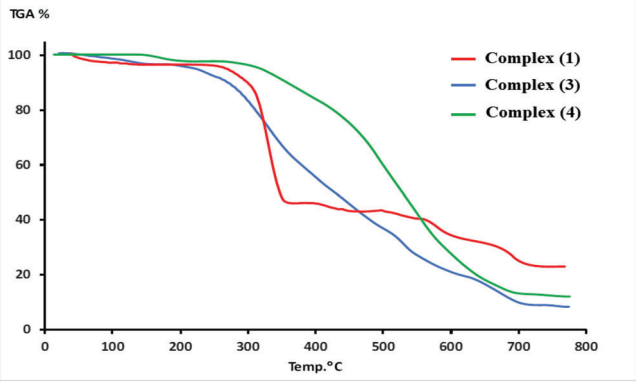

FIGURE 3 TGA of Ni (II) complexes: $[Ni_2(L^1\text{-H})(OAc)_3(H_2O)].H_2O$ (**1**), $[Ni(L^3\text{-H})_2].4H_2O$ (**3**), and $[Ni(L^4\text{-H})(OAc)(H_2O)]$ (**4**)

It is worthy to mention that the investigated complexes have considerably high thermal stability as plausibly inferred from the first decomposition DTGA peak maximum (T_m).[33] The bonding between Ni (II) ion and the ligands (L^1–L^4) starts to dissociate at T_m values of ca. 333.9, 351.5, 361.7, and 404.3°C, respectively (Table 2 and Figure 3). Accordingly, L^4 displayed the highest binding capacity with the metal ion which could be attributed to many factors as inductive effect of the substituents, bulkiness, geometry, and stoichiometry of the complex.[40] In addition, the delay of water molecules removal up to ~162°C in the case of $[Ni(L^3\text{-H})_2].4H_2O$ complex (**3**) may be related to strong hydrogen bonds formation between the outer sphere water molecules and electronegative atoms as fluorine, nitrogen, and oxygen of two ligands molecules.[40]

3.2 | Theoretical studies

3.2.1 | Chemical reactivity modeling

DFT was applied to estimate the best optimized conformations and to calculate the theoretical parameters of the synthesized compounds from which the electrophilic binding sites and the molecular activity were predicted. The theoretical data of the investigated ligands (L^1–L^4) and Ni (II) complexes (**2**) and (**4**) as illustrating examples are collected in Table 3 and Figures 4–7 and S14–S23. The calculated bond lengths and bond angles of Ni (II) complexes (**2**) and (**4**) typified square planar geometry (Table S2). Slight elongation in the bond length was noticed in N(35) = C(29), O(26)-S(25), N(14) = C(12), and N(14)-C(15) in complex (**2**) upon coordination through phenolic-O, the azomethine-N, enolic S(O)OH, and thiazole-N in tetradentate mode (Figure 4). The dihedral angles N(13)-Ni(35)-O(10), O(10)-Ni(35)-O(43), N(13)-Ni(35)-O(36), and O(36)-Ni(35)-O(43) of complex (**4**) were 94.92°, 84.41°, 90.60°, and 90.05° respectively indicating square planar geometry around the Ni (II) ion (Figure 5). The small discrepancy in coordination sphere angles than the ideal square planar supported the existence of a small tetrahedral percentage as early calculated.

Generally, small energy gap ΔE (E_{LUMO}-E_{HOMO}) is taken as a good indicator for complexation ability with neighboring central metal ion having empty d-orbital or biological receptor as well as softness and hence chemical reactivity.[19] Among the examined ligands, L^4 exhibits

TABLE 2 Thermal analyses data of Ni (II) complexes derived from L^1–L^4

Complex (M:L)	T_m °C	Temp. Range (°C)	Wt. loss/ Residue % Found	Calc.	Assignment
$[Ni_2(L^1\text{-}H)(OAc)_3(H_2O)].H_2O$ (2:1)	52.4	35.9–103.4	3.29	2.97	—Outer sphere H_2O
	201.4	103.4–309.7	12.8	12.9	—Inner sphere H_2O, $-CH_3COOH$
	333.9	309.7–373.3	37.8	59.5	—$2CH_3COOH$, Decomposition of ligand ($-C_{13}H_8N_2OS$)
	597.3	373.3–698.7	21.5		
		Residue	24.6	24.7	2NiO
$[Ni_2(L^2\text{-}H)(OAc)_3(H_2O)]$ (2:1)	143.6	73.6–296.9	11.4	11.6	—H_2O, $-CH_3COOH$
	351.5	296.9–379.6	24.4	66.1	—$2CH_3COOH$, Decomposition of ligand ($-C_{16}H_9N_3OS_2$)
	445.6	379.6–523.2	41.9		
		Residue	22.3	22.3	2NiO
$[Ni(L^3\text{-}H)_2].4H_2O$ (1:2)	139.5	34.8–162.3	7.52	7.79	—$4H_2O$
	361.7	220.5–432.6	5.92	84.1	Decomposition of ligand ($-C_{38}H_{28}F_2N_8O_5S_2$)
	545.2	432.6–698.1	78.4		
		Residue	8.12	8.07	NiO
$[Ni(L^4\text{-}H)(OAc)(H_2O)]$ (1:1)	168.4	148.2–238.4	3.10	2.92	—H_2O
	404.3	265.7–478.9	20.7	85.0	—CH_3COOH, Decomposition of ligand ($-C_{22}H_{14}FN_5O_2S_2$)
	610.5	478.9–697.6	64.2		
		Residue	12.0	12.1	NiO

TABLE 3 The molecular parameters of some selected synthesized compounds

Compound	E_T (Hartree)	D (Debye)	E_{HOMO} (eV)	E_{LUMO} (eV)	ΔE (eV)	η (eV)	S (eV^{-1})	μ (eV)	χ (eV)	ω (eV)
L^1	−1235	7.658	−6.351	−2.111	4.240	2.120	0.236	−4.231	4.231	4.222
L^2	−1803	8.197	−6.326	−2.422	3.904	1.952	0.256	−4.374	4.374	4.901
L^3	−1675	5.165	−6.383	−2.673	3.710	1.855	0.269	−4.528	4.528	5.526
L^4	−2243	4.379	−6.372	−2.669	3.703	1.852	0.270	−4.520	4.520	5.516
Complex (2)	−5581	7.989	−5.943	−3.917	2.026	1.013	0.494	−4.930	4.930	12.00
Complex (4)	−4055	4.010	−6.024	−2.616	3.408	1.704	0.293	−4.320	4.320	5.476

FIGURE 4 Optimized structure of $[Ni_2(L^2\text{-}H)(OAc)_3(H_2O)]$ complex (**2**)

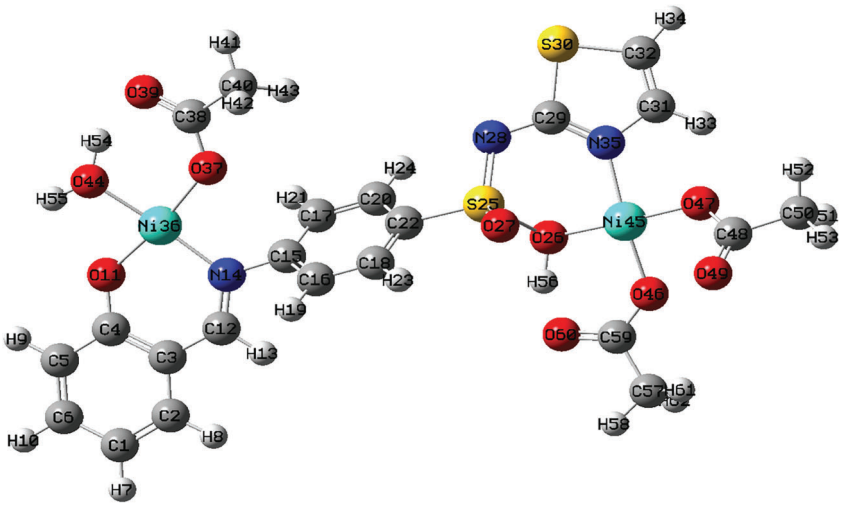

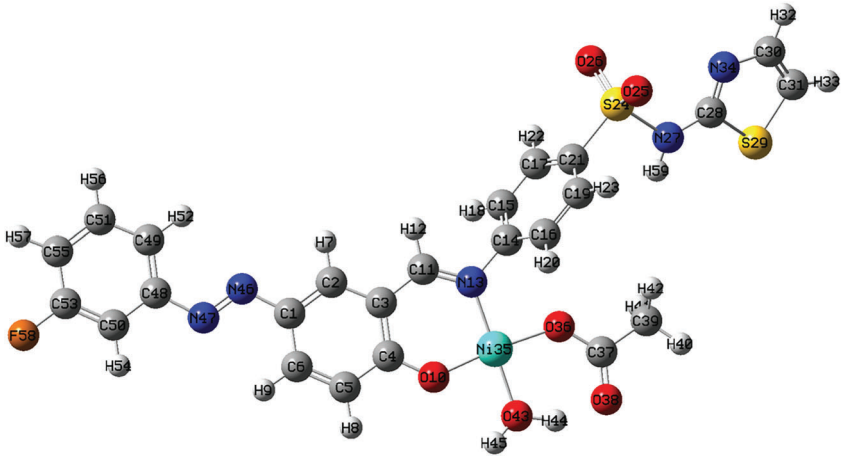

FIGURE 5 Optimized structure of [Ni(L^4-H)(OAc)(H_2O)] complex (**4**)

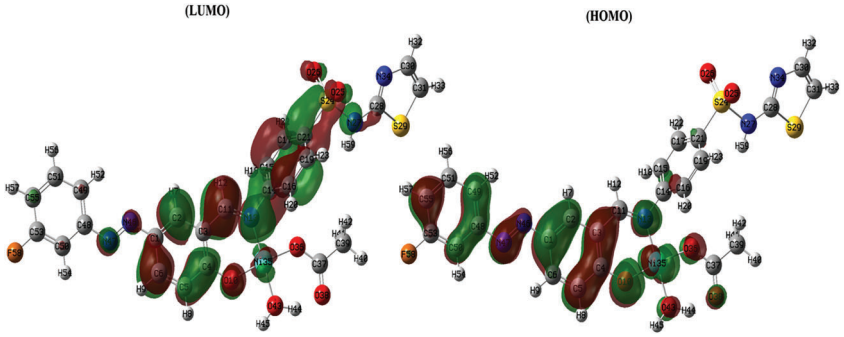

FIGURE 6 LUMO and HOMO of [Ni(L^4-H)(OAc)(H_2O)] complex (**4**)

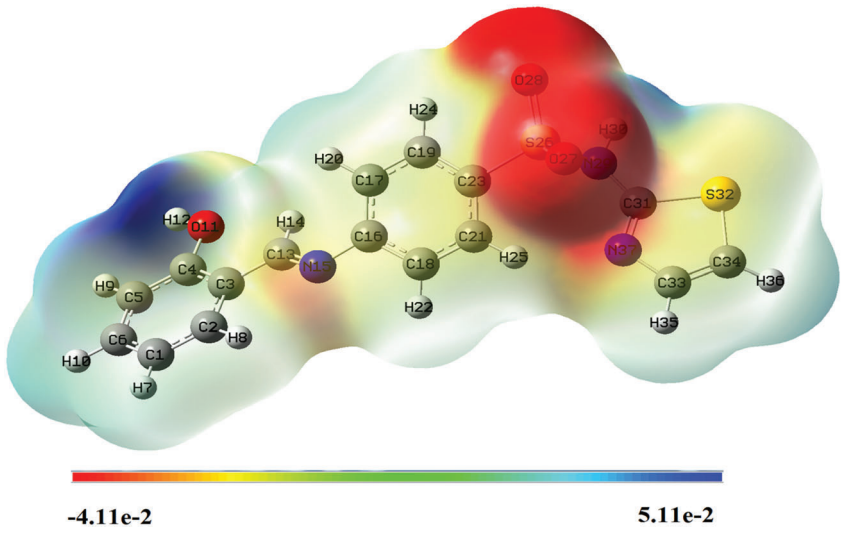

FIGURE 7 Molecular electrostatic potential of L^2

the smallest ΔE (3.70 eV) which points to an ease of electron transfer with Ni (II) d-orbitals owing to its long-conjugated system of three linked phenyl groups with several donor atoms such as oxygen, nitrogen, and sulfur (Figure 6). Also, the higher negative total energy (E_T) of the complexes (**2**) and (**4**) compared to their free ligands (Table 3) implies the greater stability of the isolated complexes. Additional molecular reactivity parameters have been estimated including, electrophilicity (ω), hardness (η), softness (S), electronegativity (χ), dipolar moment (D).[41] Apparently, there is a direct correlation between these chemical reactivity indices and different biological inhibition activities. For instance, the relatively low dipole moment values (D) for L^4 and its Ni (II) complex (**4**) suggest the feasible ability to penetrate the phospholipid bilayer of the biological cell membrane.[42]

Seemingly, L^4 displays the lowest η (1.852 eV) and highest S (0.270 eV^{-1}) and subsequently it is expected to have sufficient softness compared to other studied ligands and hence superior biological activity as confirmed practically in this research.

Moreover, the electronic charge distribution was screened theoretically on the surface of the synthesized ligands to specify the sites of interaction. The areas of high electron density, denoted in red, are intense on the sulfonamide as well as the azomethine parts of the ligands. The electron-rich regions in the case of L^2 (Figure 7) are clearly localized on the atoms N(15), N (37), and O(27) accounting for possible binding sites which is in harmony with the chelation pattern confirmed by the spectroscopic study in this contribution.

3.2.2 | Molecular docking approach

In silico investigation of the inhibition strengths of the synthesized compounds were achieved by molecular docking approach versus the 3D crystal structure of 3s7s protein. The targeted protein represents the human cytochrome P450 aromatase which catalyzes the synthesis of estrogens and is complexed with breast cancer drugs.[43] Docking results such as ligand-receptor sites, interaction type, interaction distances, internal energy (E), and scoring energy (S) are shown in Table 4 and Figures 8 and S24–S26. The effective ligand-receptor bond lengths for most of the tested compounds were ≤3.5 Å which give insight into typical real bonds and high ligand-receptor binding affinity.[17,44] For instance, the closest interaction

TABLE 4 The docking parameters of synthesized compounds against 3s7s protein

Compound	Ligand site	Receptor site	Interaction type	Distance (Å)	E (kcal/mol)	S (kcal/mol)
L^1	N 29	LEU 372	H-donor	3.13	−2.9	−6.6984
	N 29	MET 374	H-donor	3.78	−2.1	
	O 28	VAL 373	H-acceptor	3.36	−0.8	
	6-ring	LEU 477	π-H	4.39	−0.6	
L^2	S 32	MET 303	H-donor	3.73	−0.1	−7.6582
	O 28	ALA 307	H-acceptor	3.37	−0.8	
L^3	C 34	MET 311	H-donor	3.73	−0.8	−7.9185
	O 27	ARG 115	H-acceptor	3.14	−1.6	
	O 27	ARG 435	H-acceptor	3.15	−3.2	
	N 28	TRP 141	H-acceptor	3.13	−1.1	
	6-ring	ALA 438	π-H	4.43	−0.9	
L^4	O 10	MET 303	H-donor	3.14	−2.4	−9.0101
	S 44	SER 314	H-donor	3.01	−0.8	
	O 26	CYS 437	H-acceptor	3.31	−1.1	
	N 30	CYS 437	H-acceptor	3.50	−1.2	
	5-ring	VAL 370	π-H	3.91	−0.8	
Complex (1)	O 38	THR 310	H-donor	3.05	−4.5	−6.7220
	O 47	VAL 370	H-acceptor	3.24	−0.8	
	Ni 41	PRO 429	Metal	2.15	−1.1	
Complex (2)	S 32	LEU 477	H-donor	3.08	−0.4	−6.0659
	O 46	ALA 306	H-donor	3.44	−1.6	
Complex (3)	O 26	ASN 75	H-acceptor	3.13	−2.7	−7.5583
	N 29	LYS 473	H-acceptor	3.20	−1.7	
	N 30	LYS 473	H-acceptor	3.28	−1.0	
Complex (4)	C 5	MET 303	H-donor	3.51	−1.1	−9.3457
	S 29	PRO 429	H-donor	3.03	−1.3	
	O 43	ALA 306	H-donor	3.22	−1.7	
	O 43	THR 310	H-donor	2.68	−9.3	
	5-ring	VAL 370	π-H	3.64	−1.1	

as H-donors is observed with Serine SER 314 (3.01 Å) and Threonine THR 310 (2.68 Å) amino acids in the case of L^4 and its complex (**4**), respectively. In addition, the ligand-protein binding affinities were predicted from the scoring energy function based on parameters such as intermolecular hydrogen bonds, van der Waals interaction, deformation effect, hydrophobic interaction, and entropy.[45] So, all ligands show an extent of inhibition to the 3s7s protein following the order $L^4 > L^3 > L^2 > L^1$ which could be related to an increase in the synergistic properties by a consortium of different bioactive moieties such as azomethine, sulfonamide, thiazole ring, 3-fluorophenylazo substituent ongoing from L^1 to L^4. Remarkably, the binding sites of L^4 are O(10), S(44), (O (26) and N(30)), and the five-ring sites with the Methionine MET 303, Serine SER 314, Cysteine CYS 437, and Valine VAL 370 amino acids (Figure 8), respectively, with relatively highest negative scoring energy (−9.0101 kcal/mol) (Table 4). The negative value for energies for all tested compounds means spontaneous binding of the ligand to the target receptor without requiring energy. Likewise, the highest inhibition activity and the most stable interaction with the 3s7s protein among the Ni (II) complexes was discerned for complex (**4**) with a scoring energy of −9.3457 kcal/mol. Furthermore, the surface mapping of the ligands-protein pockets (Figures 8 and S24–S26) demonstrated strong interaction between the protein and the synthesized compounds as the ligands appeared completely implanted in the cavity of the surrounded amino acids.

3.3 | Biological activity studies

3.3.1 | Antibacterial and antifungal activities

The in vitro antimicrobial assessment of the sulfonamide-based Schiff bases (L^1–L^4) revealed varying inhibitory actions as shown in Table 5. MIC values expressed in μM, have been estimated only for the tested compounds of

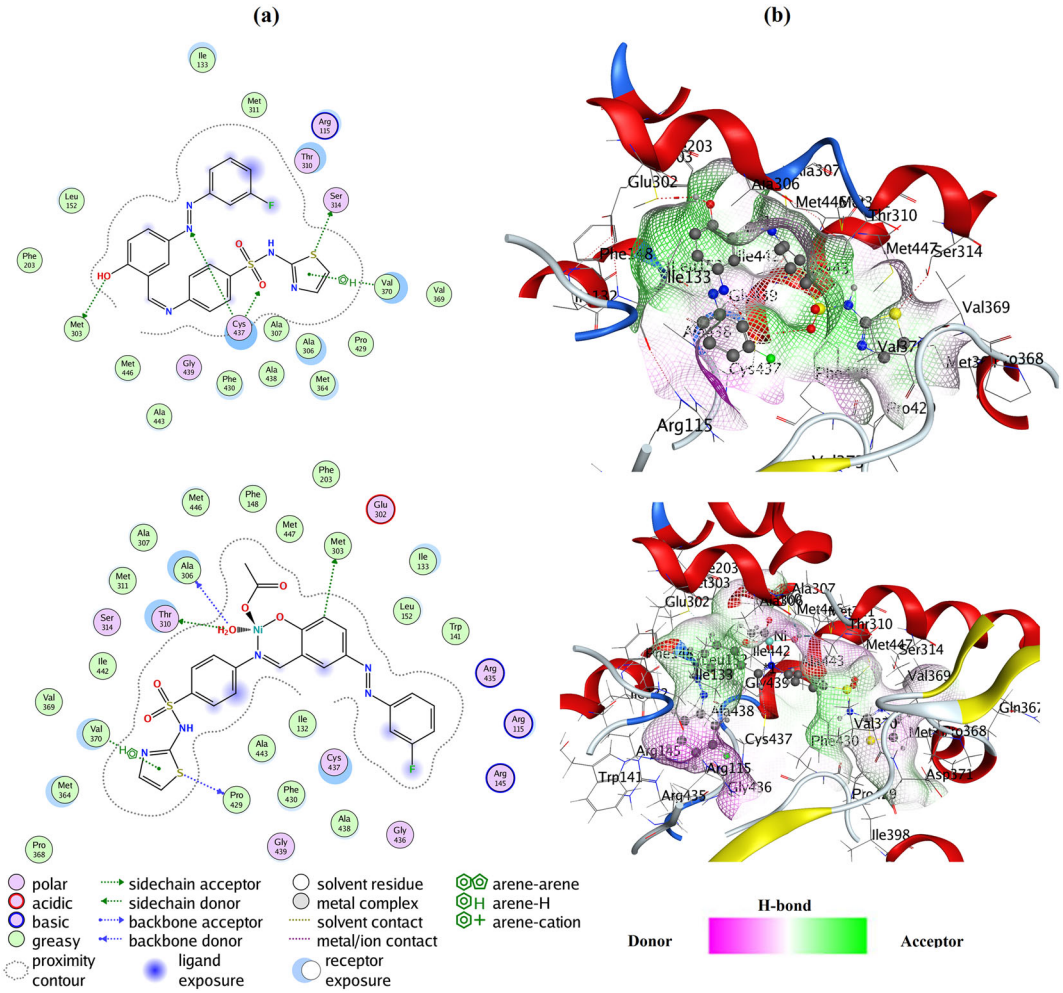

FIGURE 8 Binding features (a) surface maps (b) of the best docked poses of the synthesized L^4 and complex (**4**) against breast cancer protein 3s7s

TABLE 5 Antibacterial and antifungal inhibition zone in mm and MIC (μM) of the synthesized Schiff bases

	Gram-positive bacteria		Gram-negative bacteria		Fungi	
Compound	***S. pneumoniae***	***B. subtilis***	***P. aeruginosa***	***E. coli***	***A. fumigatus***	***C. albicans***
L^1	17.3 ± 0.6 (113.1)	20.2 ± 0.4 (14.1)	NA[a]	15.9 ± 0.4 (226.2)	19.8 ± 0.3 (28.3)	NA
L^2	16.9 ± 0.4 (86.9)	19.3 ± 0.3 (21.7)	NA	14.9 ± 0.4 (> 500)	17.9 ± 0.4 (86.9)	NA
L^3	20.6 ± 0.6 (4.89)	22.4 ± 0.4 (2.46)	NA	16.9 ± 0.6 (78.4)	20.3 ± 0.3 (9.79)	NA
L^4	19.6 ± 0.6 (16.2)	20.0 ± 0.3 (8.10)	NA	15.9 ± 0.5 (129.8)	21.4 ± 0.6 (4.05)	NA
Ampicillin	23.8 ± 0.20 (2.80)	26.4 ± 0.5 (1.40)	NT[b]	NT	NT	NT
Gentamycin	NT	NT	17.3 ± 0.1 (32.7)	19.9 ± 0.3 (8.17)	NT	NT
Amphotericin B	NT	NT	NT	NT	23.7 ± 0.1 (2.11)	25.4 ± 0.1 (1.06)

[a]No activity.
[b]Not tested.

TABLE 6 Cytotoxicity activity (IC_{50}) in μM of Schiff bases and some of their complexes

	Tumor cell lines			
Compounds	**HCT-116**	**MCF-7**	**HepG-2**	**Normal cell line OEC**
L^1	25.3 ± 0.9	41.3 ± 1.3	53.2 ± 1.6	NT
L^2	29.5 ± 0.9	40.6 ± 1.1	50.6 ± 1.5	74.6 ± 5.4
L^4	7.98 ± 0.6	12.3 ± 0.8	16.0 ± 0.7	>100
Complex (1)	92.1 ± 2.8	>100	>100	49.8 ± 4.4
Complex (2)	37.0 ± 1.4	41.9 ± 1.8	71.5 ± 2.8	86.3 ± 6.9
Complex (4)	44.1 ± 1.5	37.5 ± 1.2	40.3 ± 1.3	>100
Cisplatin	8.10 ± 0.7	19.0 ± 2.3	12.2 ± 0.6	
Imatinib	19.6 ± 1.9	49.8 ± 2.3	38.2 ± 2.1	

inhibition zone growth above 6 mm. From the data, Schiff base L^4 exposed the highest antifungal activity against *Aspergillus fumigates* (MIC 4.05 μM) which is nearly 50% less potent than amphotericin B. Likewise, L^3 exhibited the most significant action against Gram-positive bacteria *S. pneumoniae* (MIC 4.89 μM) and *B. subtilis* (MIC 2.46 μM) which is about twofold less effective than ampicillin as a standard drug. These superior activities of L^3 and L^4 in comparison to L^1 and L^2 could be related to the presence of electron withdrawing group (3-fluorophenylazo) in their structures. In general, the insertion of substituents with different inductive effect and bulkiness had been proved to be effective (positively or negatively) on the antimicrobial activity of many compounds and should be considered in designing any novel drugs.[46,47] Nevertheless, all studied ligands showed negligible to mild activities versus Gram-negative germs (*P. aeruginosa* and *E. coli*) in contrast to Gram-positive ones (Table 5) reflecting the cell wall structure as an additional prominent factor in controlling the inhibition.[48] Clearly, the absence of the outer lipid membrane in Gram-positive strain wall makes it more vulnerable to be attacked by the tested compounds despite its thicker peptidoglycan layer.

3.3.2 | Cytotoxicity assessment

The antiproliferative potency for some selected Schiff base ligands and their Ni (II) complexes has been screened as presented in Table 6 and Figures 9, 10, and S27–S31. There is an apparent steady trend in the IC_{50} values for the investigated ligands (Figure 9) and their Ni (II) complexes (Figure 10). All compounds were designed to possess in their structure benzenesulfonamide group as a basic unit which is known to impose DNA damage and hence cell death via apoptosis.[49] In addition, the ligand modification by inserting other bioactive substituents to the benzenesulfonamide group would facilitate its propensity for DNA-binding through hydrogen bonds. Based on IC_{50} values in μM, it is evident that L^4 has the prominent activity against the three cancer cell lines HCT-116 (7.98 μM), MCF-7 (12.3 μM), and HepG-2 (16.0 μM). These low values indicate anticancer

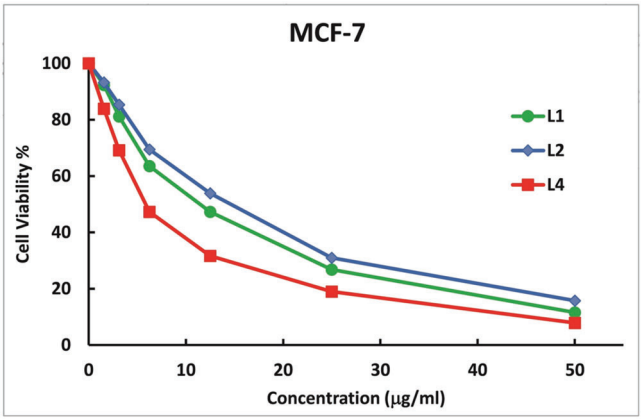

FIGURE 9 The inhibitory dose response curves of some selected ligands against MCF-7

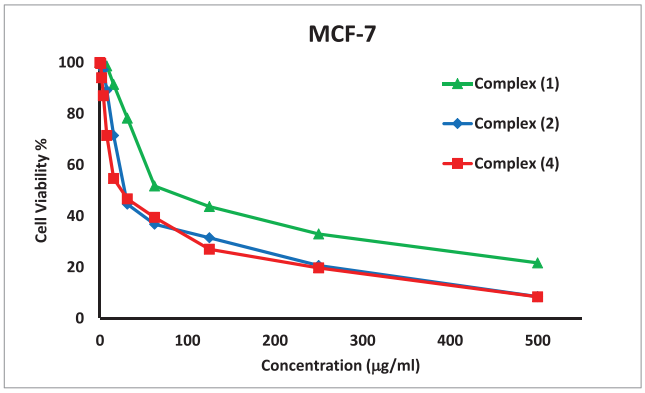

FIGURE 10 The inhibitory dose response curves of some selected complexes against MCF-7

equipotency impact of L^4 in comparison with cisplatin as a reference control (Table 6). Similarly, complex (**4**) as well as complex (**2**) exhibit about onefold and/or twofold less antiproliferative action versus the three tested cell lines relative to imatinib as an effective drug. The preceding findings are matched to great extent with the predicted ones from the docking simulations.

Further, L^4 and its Ni (II) complex (**4**) show insignificant toxicity on normal oral epithelial cell line (OEC) when compared to other studied compounds as depicted in Table 6 and Figure S31. Ultimately, the synthesized Schiff base L^4 and its Ni (II) complex, [Ni(L^4-H)(OAc)(H_2O)], seem to possess promising therapeutic effect as antitumor candidates after additional preclinical examinations.

4 | CONCLUSION

In this research, four sulfonamide Schiff bases (L^1–L^4) and their novel Ni (II) complexes as possible non-platinum therapeutic drugs were synthesized, characterized and examined for their biological activities. The mass spectral data of complexes (**1**) to (**4**) displayed molecular ion peaks ($M^{+\bullet}$) that support plentifully their proposed chemical structures. Also, the thermal decomposition steps of all complexes confirmed their high thermal stability. Besides, the slight difference in coordination sphere angles from the ideal square planar supported the existence of a small tetrahedral percentage (N_t) as calculated from magnetic measurement and illustrated by the DFT-B3LYP/6-31G method. The docking simulation outcomes predicted a good propensity to bind with the breast cancer protein 3s7s in the case of L^4 and its complex (**4**) that is in accord with their recorded antiproliferative potencies. Further preclinical inspections including intracellular ROS generation, ADMET-score, clinical trials, and drug approval process should be done on the most promising chemotherapeutic candidates such as L^4 and [Ni(L^4-H)(OAc)(H_2O)].

ACKNOWLEDGMENTS

The authors would like to express their gratitude to Alexandria University, Alexandria, Egypt for providing administrative and technical support.

DATA AVAILABILITY STATEMENT

The data that support the findings of this study are available in the supplementary material of this article.

ORCID

Ahmed M. Ramadan https://orcid.org/0000-0002-4815-1487

Hoda A. Bayoumi https://orcid.org/0000-0001-7423-7359

Rehab M. I. Elsamra https://orcid.org/0000-0003-1217-748X

REFERENCES

[1] R. Paulpandiyan, N. Raman, *J. Mol. Struct.* **2016**, *1125*, 374.

[2] S. Omidi, A. Kakanejadifard, *RSC Adv.* **2020**, *10*, 30186.

[3] M. N. Uddin, S. S. Ahmed, S. M. R. Alam, *J. Coord. Chem.* **2020**, *73*, 3109.

[4] R. M. El-Ferjani, M. Ahmad, S. M. Dhiyaaldeen, F. W. Harun, M. Y. Ibrahim, H. Adam, B. M. Yamin, M. M. J. Al-Obaidi, R. Al Batran, *Sci. Rep.* **2016**, *6*, 38748.

[5] H. Kaur, S. M. Lim, K. Ramasamy, M. Vasudevan, S. A. A. Shah, B. Narasimhan, *Arab. J. Chem.* **2020**, *13*, 377.

[6] G. Devagi, F. Dallemer, P. Kalaivani, R. Prabhakaran, *J. Organomet. Chem.* **2018**, *854*, 1.

[7] S. H. Sumrra, A. U. Hassan, M. Imran, M. Khalid, E. U. Mughal, M. N. Zafar, M. N. Tahir, M. A. Raza, A. A. C. Braga, *Appl. Organomet. Chem.* **2020**, *34*, e5623.

[8] S. Mondal, T. K. Mondal, Y. Rajesh, M. Mandal, C. Sinha, *Polyhedron* **2018**, *151*, 344.

[9] R. Shah, H. Katouah, A. A. Sedayo, M. Abualnaja, M. M. Aljohani, F. Saad, R. Zaky, N. M. El-Metwaly, *J. Mol. Liq.* **2020**, *319*, 114116.
[10] E. R. Jamieson, S. J. Lippard, *Chem. Rev.* **1999**, *99*, 2,467.
[11] A. M. Ramadan, A. A. Alshehri, S. Bondock, J. Saudi, *Chem. Soc.* **2019**, *23*, 1192.
[12] S. Parveen, *Appl. Organomet. Chem.* **2020**, *34*, e5687.
[13] M. B. Alshammari, M. Ramadan, A. A. Aly, E. M. El-Sheref, M. A. Bakht, M. A. A. Ibrahim, A. M. Shawky, *J. Mol. Struct.* **2021**, *1*, 230, 129649.
[14] G. H. Jeffery, J. Bassett, J. Mendham, R. C. Denney, *Vogel's Textbook of Quantitative Chemical Analysis*, John Wiley & Sons, Inc, NY **1989**.
[15] R. Dennington, T. Keith, J. Millam, *Gauss View, Version 4.1.2*, Semichem Inc, Shawnee Mission, KS **2007**.
[16] K. R. Valasani, J. R. Vangavaragu, V. W. Day, S. S. Yan, *J. Chem. Inf. Model.* **2014**, *54*, 902.
[17] R. Shah, T. M. Habeebullah, F. Saad, I. Althagafi, A. Y. Al-dawood, A. M. Al-Solimy, Z. A. Al-Ahmed, F. Al-Zahrani, T. A. Farghaly, N. El-Metwaly, *Appl. Organomet. Chem.* **2020**, *34*, e5886.
[18] S. M. Gomha, I. M. Abbas, M. A. A. Elneairy, M. M. Elaasser, B. K. A. Mabrouk, *J. Serb. Chem. Soc.* **2015**, *80*, 1,251.
[19] A. M. Ramadan, R. M. I. Elsamra, S. Bondock, *Appl. Organomet. Chem.* **2021**, *35*, e6102.
[20] M. S. Masoud, S. A. A. El-Enein, A. E. Ali, E. H. A. Elhamed, *J. Mol. Struct.* **2020**, *1*, 202, 127172.
[21] A. I. Vogel, *A Text-Book of Practical Organic Chemistry*, Third ed., Longmans, London **1961**.
[22] Y. Cui, X. Dong, Y. Li, Z. Li, W. Chen, *Eur. J. Med. Chem.* **2012**, *58*, 323.
[23] R. R. Coombs, M. K. Ringer, J. M. Blacquiere, J. C. Smith, J. S. Neilsen, Y. -S. Uh, J. B. Gilbert, L. J. Leger, H. Zhang, A. M. Irving, S. L. Wheaton, C. M. Vogels, S. A. Westcott, A. Decken, F. J. Baerlocher, *Transition Met. Chem.* **2005**, *30*, 411.
[24] P. Nagpal, R. V. Singh, *Appl. Organomet. Chem.* **2004**, *18*, 221.
[25] G. Valarmathy, R. Subbalakshmi, R. Sumathi, R. Renganathan, *J. Mol. Struct.* **2020**, *1*, 199, 127029.
[26] E. H. Alosaimi, A. A. Alsibaai, M. S. El-Shahawi, M. S. Refat, *Russ. J. Phys. Chem. A* **2018**, *92*, 2227.
[27] A. M. A. Alaghaz, R. A. A. Ammar, G. Koehler, K. P. Wolschann, T. M. El-Gogary, *Spectrochim. Acta Part a* **2014**, *128*, 724.
[28] C. M. Sharaby, M. F. Amine, A. A. Hamed, *J. Mol. Struct.* **2017**, *1134*, 208.
[29] S. Hamura, T. Oda, Y. Shimizu, K. Matsubara, H. Nagashima, *J. Chem. Soc., Dalton Trans.* **2002**, 1521.
[30] G. Prajapat, R. Gupta, N. Bhojak, *Orient. J. Chem.* **2019**, *35*, 308.
[31] A. Z. El-Sonbati, M. A. Diab, S. M. Morgan, A. M. Eldesoky, M. Z. Balboula, *Appl. Organomet. Chem.* **2018**, *32*, e4207.
[32] M. Ul-Hassan, A. Scozzafava, Z. H. Chohan, C. T. Supuran, *J. Enzyme Inhib.* **2001**, *16*, 499.
[33] A. M. A. Alaghaz, H. A. Bayoumi, Y. A. Ammar, S. A. Aldhlmani, *J. Mol. Struct.* **2013**, *1035*, 383.
[34] H. M. Abumelha, J. H. Al-Fahemi, I. Althagafi, A. A. Bayazeed, Z. A. Al-Ahmed, A. M. Khedr, N. El-Metwaly, *J. Inorg. Organomet. Polym. Mater.* **2020**, *30*, 3277.
[35] J. McKnight, M. R. Cheesman, A. J. Thomson, J. S. Miles, A. W. Munro, *Eur. J. Biochem.* **1993**, *213*, 683.
[36] A. M. Mansour, O. R. Shehab, *Arabian J. Chem.* **2021**, *14*, 102,932.
[37] N. Al-Awadi, N. M. Shuaib, A. El-Dissouky, *Spectrochim. Acta Part a* **2006**, *65*, 36.
[38] A. Ashraf, W. A. Siddiqui, J. Akbar, G. Mustafa, H. Krautscheid, N. Ullah, B. Mirza, F. Sher, M. Hanif, C. G. Hartinger, *Inorg. Chim. Acta* **2016**, *443*, 179.
[39] H. Moustafa, G. G. Mohamed, S. Elramly, *J. Chin. Chem. Soc.* **2020**, *67*, 1783.
[40] X.-Q. Song, Y.-Q. Peng, G.-Q. Cheng, X. -R. Wang, P. -P. Liu, W. -Y. Xu, *Inorg. Chim. Acta* **2015**, *427*, 13.
[41] R. K. Ray, G. R. Kauffman, *Inorg. Chim. Acta* **1990**, *173*, 207.
[42] M. D. L. A. Zermeño-Macías, M. M. González-Chávez, F. Méndez, R. González-Chávez, A. Richaud, *Molecules* **2017**, *22*, 427.
[43] D. Ghosh, J. Lo, D. Morton, D. Valette, J. Xi, J. Griswold, S. Hubbell, C. Egbuta, W. Jiang, J. An, H. M. L. Davies, *J. Med. Chem.* **2012**, *55*, 8,464.
[44] R. C. Wade, P. J. Goodford, *Prog. Clin. Biol. Res.* **1989**, *289*, 433.
[45] J. de Azevedo, F. Walter, R. Dias, *Curr. Drug Targets* **2008**, *9*, 1031.
[46] W. Al Zoubi, A. A. S. Al-Hamdani, S. D. Ahmed, Y. G. Ko, *Appl. Organomet. Chem.* **2018**, *32*, e3895.
[47] S. Narwal, S. Kumar, P. K. Verma, *Chem. Cent. J.* **2017**, *11*, 52.
[48] N. Raman, R. Jeyamurugan, S. Sudharsan, K. Karuppasamy, L. Mitu, *Arabian J. Chem.* **2013**, *6*, 235.
[49] M. González-Álvarez, A. Pascual-Álvarez, L. del Castillo Agudo, A. Castiñeiras, M. Liu-González, J. Borrása, G. Alzuet-Piña, *Dalton Trans.* **2013**, *42*, 10244.

SUPPORTING INFORMATION

Additional supporting information may be found in the online version of the article at the publisher's website.

How to cite this article: A. M. Ramadan, H. A. Bayoumi, R. M. I. Elsamra, *Appl Organomet Chem* **2021**, e6412. https://doi.org/10.1002/aoc.6412